Available online at www.sciencedirect.com
SCIENCE DIRECT
ELSEVIER
Journal of the European Ceramic Society 25 (2005) 2799–2803
JECS
www.elsevier.com/locate/jeurceramsoc

Selfconsistent electrical charging in insulators

H.-J. Fitting [a,*], X. Meyza [b], C. Guerret-Piécourt [c], C. Dutriez [d], M. Touzin [b], D. Goeuriot [b], D. Tréheux [d]

[a] *Physics Department, University of Rostock, Universitätsplatz 3, D 18051 Rostock, Germany*
[b] *Centre Sciences des Matériaux et des Structures, Ecole Nationale Supérieure des, Mines, 158 cours Fauriel, F-42023 Saint-Etienne Cedex 2, France*
[c] *Laboratoire de Physico-Chimie des Polymeres, UMR-CNRS 5067, Université de, Pau, BP 1157, F-64013 Pau Cedex, France*
[d] *Laboratoire d'Ingénierie et Fonctionnalisation des Surfaces, UMR-CNRS 5621, Ecole Centrale de Lyon, 36 avenue Guy de Collongue, F-69134 Ecully Cedex, France*

Available online 5 April 2005

Abstract

A Monte Carlo program based on acoustic and optical phonon scattering as well as on impact ionisation of valence band electrons has advantages in description of very low energy electron scattering (in eV and meV regions) and is aimed especially to wide gap dielectrics and insulators. Thus, the rapid relaxation and the ballistic transport of excited electrons within the conduction band of a wide gap insulator occurs over femtoseconds. The field-dependent transport and trapping parameters allow us to model the selfconsistent charge transport and charging-up of SiO_2 thin layers as well as bulk Al_2O_3 samples during electron bombardment. The resulting distributions of currents, charges and electric fields within these samples explain, e.g. the phenomena of field-enhanced and field-blocked secondary electron emission. In order to prove the accessible quantity of the surface charging-up potential we have chosen the X-ray bremsstrahlung (BS) spectra, i.e. the shift of the short wavelength threshold due to the negative surface potential V_0 and respective retarding of the incident electron beam. This effect is demonstrated for a 3 mm bulk Al_2O_3 sample and $E_0 = 30$ keV electron beam irradiation resulting in a huge negative surface potential of $V_0^{\mathrm{exp}} = -17$ kV.
© 2005 Elsevier Ltd. All rights reserved.

Keywords: Dielectric properties; Electrical properties; Al_2O_3; SiO_2; Insulators

1. Introduction

The investigation of dielectric polarization and its influence on the essential features of insulating materials has led finally to better understanding and applications of these materials, see e.g. the conference series on electric charges in non-conductive materials[1] and ref. 2. One of the subjects of interest is the prediction of electrical charging of insulators under electron beam irradiation as it is of great importance in electron spectroscopy and microscopy and many fields of modern technology. For instances, the knowledge of such phenomena would help in preventing insulator breakdown mainly responsible for the damage of electronic devices.[3,4]

For description of the charge transport the phonon-based model of low energy scattering within an energy band structure of a solid bears certain advantages against common free-electron scattering mechanisms. However, the latter ones describe the inelastic processes as well, but the main improvement is given by introducing the acoustic phonon scattering instead of the elastic binary encounter approximation of the Mott scattering for electrons with low energies $E < 100$ eV.[5,6] The very low energy electrons should behave like Bloch electrons and will interact with perturbations of the atomic lattice, i.e. with phonons.

With these scattering parameters we have performed the simulation of secondary electron (SE) excitation and emission from the insulator SiO_2.[6] There is a rapid impact ionization cooling leading to cascading at the beginning during the first femtoseconds followed by slower attenuation due to LO phonon emission losses. Respective electron trajectories

* Corresponding author. Tel.: +49 381 498 6760; fax: +49 381 498 6802.
E-mail address: hans-joachim.fitting@physik.uni-rostock.de (H.-J. Fitting).

0955-2219/$ – see front matter © 2005 Elsevier Ltd. All rights reserved.
doi:10.1016/j.jeurceramsoc.2005.03.143

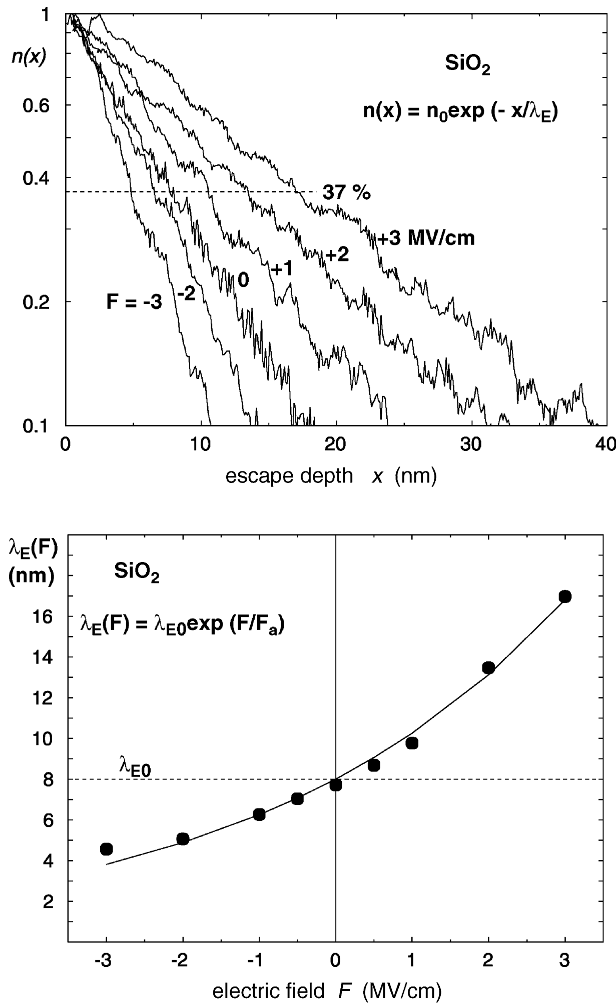

Fig. 1. Semi-logarithmic plot of the SE escape probabilities $n(x)$ in dependence on the electric field strength $F \gtrless 0$ (above); the probability 37% indicates the mean escape depth $\lambda_e(F)$ as a function of the field which is plotted below and fitted by the formula inserted.

demonstrate the relatively short range of primary electrons PE with energies $E > 50$ eV due to strong impact ionization losses (cascading) and the much greater range of secondary electrons SE with $E < 50$ eV finally caused by the less effective phonon losses (attenuation) in a wide gap insulator like SiO_2 with $E_g = 9$ eV. By means of these MC calculations we got the electron backscattering ratio $\eta(E_0)$, the primary electron maximum range $R(E_0)$, the secondary electron yield $\delta(E_0)$, as well as the SE escape depths $\lambda(F)$ in dependence on the present electric field F.

The field-dependent transport parameters (see e.g. Fig. 1) allow us to model the selfconsistent charge transport and charging-up of insulating SiO_2 layers[7] and bulk Al_2O_3 samples[8] during electron bombardment maintained by the current components of primary electrons j_{PE}, secondary electrons j_{SE}, associated ballistic holes j_{BH} as well as Fowler–Nordheim (FN) injection j_{FN} from the substrate, see Fig. 2. The resulting distributions of all currents $j(x, t)$, charges $\rho(x, t)$, electric fields $F(x, t)$ and the potential $V(x, t)$, in dependence on the layer depth x and the time t explain the phenomena of field-blocked and field-enhanced secondary electron emission rates $\delta \gtrless 1$ and the surface potential V_0 due to the charging.

2. Current attenuation and transport

Electron beam irradiation on non-conductive samples in a scanning electron microscope (SEM) will produce internal and external currents as given in Fig. 2 as well as charge $\rho(x)$ and associated field $F(x)$ distributions.[7,8]

Therefore we have introduced the ballistic current attenuation probability W_F. First of all, W_F will depend on the actual field strength F enhancing or diminishing the mean attenuation length $\lambda(F)$, see Fig. 1. This very important transport parameter has been investigated experimentally[9] as well as calculated by Monte Carlo simulations.[6] Thus, the field-dependent attenuation probability indicated for electrons by (E) in transmission (T) and reverse (R) direction is:

$$ {}^{R}_{T}W_{EF} = \exp\left[-\frac{\Delta x}{\lambda_E(\pm F)}\right] \exp\left[-\frac{\Delta x}{\lambda_{E,0}\exp(\pm\beta_E F)}\right]. \quad (1a) $$

For holes (H) we can write the respective relation:

$$ {}^{R}_{T}W_{HF} = \exp\left[-\frac{\Delta x}{\lambda_H(\mp F)}\right] = \exp\left[-\frac{\Delta x}{\lambda_{H,0}\exp(\mp\beta_E F)}\right], \quad (1b) $$

including the mean field-dependent attenuation length λ_E for electrons and λ_H for holes with their field-free values $\lambda_{E,0}$ and $\lambda_{H,0}$ as well as the field-enhancing factors β_E and β_H, respectively.[7,8]

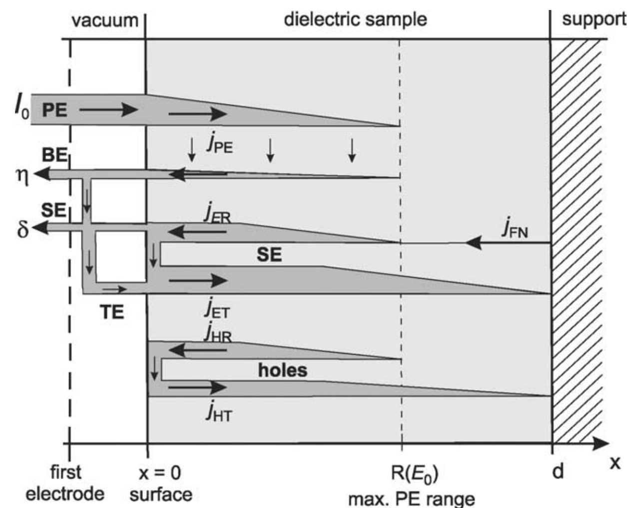

Fig. 2. Scheme of currents in an insulating sample of thickness d during electron irradiation with primary electrons (PE). The currents of inner secondary electrons (SE) and holes (H) are given in foreward (T: transmission) and in reverse (R) direction. The total re-emission fraction $\sigma = \eta + \delta$ of backscattered electrons (BE) and SE is diminished by tertiary electrons (TE). j_{FN}: Fowler–Nordheim injection of electrons from the substrate in case of strong positive charging and thin layers $d < 200$ nm, see Fig. 3.

Whereas the mean attenuation length for electrons $\lambda_E(\pm F)$ is enhanced for positive fields $F > 0$ in reverse (R) motion towards the surface, it is diminished for transmission (T) direction towards the sample support. Negative fields $F < 0$ will result in opposite relations for electrons, i.e. enhancement in (T) and retarding in (R) direction, respectively. Of course, for holes (H) the relations for ${}^{R}_{T}W_{HF}$ in Eq. (1b) should be given vice versa, i.e. with an opposite sign with respect to electrons in Eq. (1a).

Further on, we should consider electron–hole recombination as a second kind of current attenuation. With the related recombination cross sections $S_{EH} = S_{HE}$, we can write the recombination probability for electrons (E) and holes (H) over the distance Δx:

$$W_{EH} = \exp\left[-\frac{\rho_H}{e_0} S_{EH}\,\Delta x\right] \tag{2a}$$

$$W_{HE} = \exp\left[-\frac{\rho_E}{e_0} S_{HE}\,\Delta x\right]. \tag{2b}$$

Now the charges are registered separately for electrons ρ_E and for holes ρ_H, respectively.

Another attenuation of the currents is given by the trapping probability to localized electron and hole states (traps) with an overall concentration $N_{E,0}$ and an actual occupation N_E for electrons and $N_{H,0}$ and N_H for holes:

$$W_{EE} = \exp\{-[N_{E,0} - N_E(x)]\, S_{EE}\,\Delta x\} \tag{3a}$$

$$W_{HH} = \exp\{-[N_{H,0} - N_H(x)]\, S_{HH}\,\Delta x\} \tag{3b}$$

S_{EE} and S_{HH} hold for the capture cross sections for electrons and holes, respectively.

Finally, we can write the current balance in the depth x explicitely for electrons (E) in reverse (R) and transmission (T) direction:

$$j^{ER}_{ET}(x) = \left[\underbrace{j^{ER}_{ET}(x \pm \Delta x)}_{\text{convection}} + \underbrace{\frac{1}{2}(j_0 g_i(x)\,\Delta x)}_{\text{generation}}\right] \underbrace{W_{EF} W_{EH} W_{EE}}_{\text{attenaution}}, \tag{4a}$$

as well as for holes (H):

$$j^{HR}_{HT}(x) = \left[j^{HR}_{HT}(x \pm \Delta x) + \frac{1}{2}(j_0 g_i(x)\,\Delta x)\right] W_{HF} W_{HE} W_{HH}, \tag{4b}$$

with the respective expressions for the different kinds of attenuation from Eqs. (1)–(3).

2.1. Total current and field

The overall current $j(x)$ in the depth x is given by summation of the several components of Fig. 2: incident primary electrons (PE), excited inner secondary electrons (E) as well as holes (H):

$$j(x) = -j_{PE}(x) - j_{ET}(x) + j_{ER}(x) + j_{HT}(x) - j_{HR}(x) \tag{5}$$

resulting in the positive sign for positive charges moving in x-direction, i.e. transmission. This current can be inserted into the continuity equation, providing the excessive charge $\Delta\rho(x)$ as well as via the Poisson equation the respective field distribution $F(x)$, and the potential slope $V(x)$, see refs. 7, 8 In this way we obtain the selfconsistent charging process in non-conductive samples under electron irradiation.

3. Charging and secondary electron emission (SEE)

From the current $j(x, t)$ and potential $V(x, t)$ distributions of the previous part, we may deduce the respective secondary electron emission rate $\sigma(t)$ as well as the surface potential $V_0(t) = V(x = 0, t)$. Both quantities are experimentally accessible from outside the sample and can be proved directly by measurements.[10]

The total SE rate σ is given by backscattered (BE) electrons as well as by "true" secondary (SE) electrons released from the target material:

$$\sigma = \eta + \delta = \frac{I_{BE} + I_{SE}}{I_0} = \frac{I_0 + I(x < 0)}{I_0} = 1 + \frac{I(x < 0)}{I_0} \tag{6}$$

where $I(x < 0)$ is the "resulting" electron current into the vacuum diminished, of course, by the impinging reverse moving PE beam current I_0. So we have to add again I_0 to $I(x < 0)$ in order to get the real emission current ($I_{BE} + I_{SE}$) and the respective fractions ($\sigma + \delta$).

Fig. 3 shows the experimental SEE rates $\sigma(E_0, d)$ from thin SiO_2 layers on Si substrate in dependence on the layer thickness d and the incident electron beam energy E_0. We observe field-enhanced ($E_0 < 2$ keV, $d < 180$ nm) as well as field-blocked ($\sigma = 1, d < 1000$ nm) SEE.[10] The stationary final currents inside a 100 nm SiO_2 layer for $E_0 = 1$ keV are given in the lower part of Fig. 3. Obviously, the field enhanced SEE, here with $\sigma = \eta + \delta \approx 1.6$, is maintained by Fowler–Nordheim tunneling electron injection from the substrate due to the high positive charging of the near-surface region.

Contrary behavior, a blocked SEE we observe in bulk Al_2O_3 samples (Fig. 4). Respective current-charge-field-potential distributions inside bulk Al_2O_3 samples with their time (t) and energy (E_0) dependences we have calculated in ref. 8

Thus, we may observe the time dependence of the secondary emission $\sigma(t)$ presented in Fig. 4 (above). The positive charging at $E_0 = 1$ keV is limited by the surrounding grid potential V_G. On the other hand, the negative charging at $E_0 = 30$ keV is not limited by returning SE (or TE), even SE are enforced to leave the negative surface, and the surface potential approaches a high negative saturation with $V_0 \approx -21$ V after $t \geq 20$ ms. Of course, this huge negative charging has led to a retarding of the primary electron beam. This retarding of incident PE is correlated with a decrease of the maximum electron range $R(E'_0)$ within the insulating sample, finally leading to $\sigma(E'_0) \rightarrow 1$.

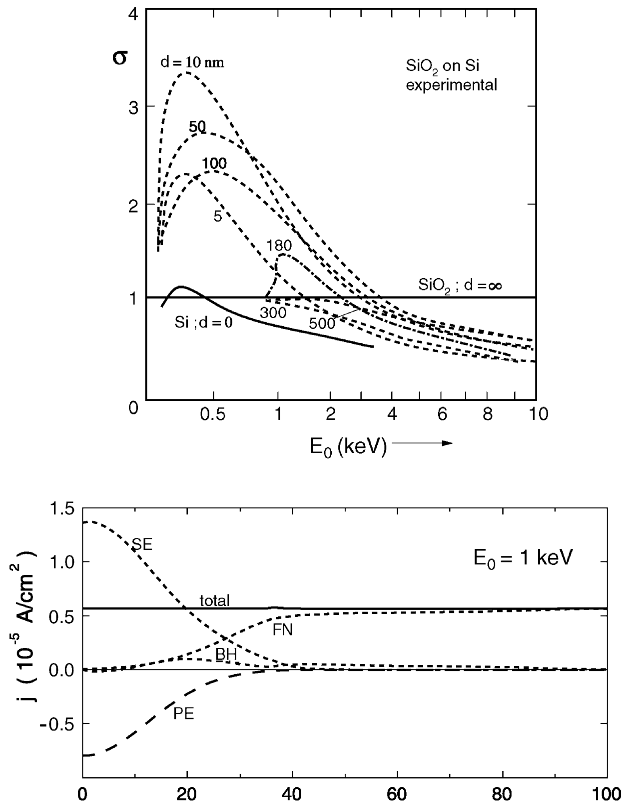

Fig. 3. Experimental SE emission rates σ in dependence on PE initial energies E_0 and SiO_2 layer thickness d (above); current components of the steady-state secondary electron emission from a 100 nm SiO_2 layer under electron irradiation of $E_0 = 1$ keV (below); PE: primary electrons, SE: secondary electrons, BH: ballistic holes, FN: Fowler–Nordheim tunneling injection. The resulting total current in the steady state remains constant: $j_{tot}(x, t) = \text{const}$.

Let us look to the influence of the grid potential V_G (hitherto we have considered only a grounded grid with $V_G = 0$). In Fig. 4 (above) we see a drastic change of the σ-slope with time when increasing the grid potential V_G to +10 V, +100 V, and +1000 V. Now, obviously, the surface will be charged more positively and it takes more time until the surface potential V_0 is reaching the positive grid potential V_G and starting the retarding process.

Indeed, when looking to the time-dependent and final steady state charge distributions in Fig. 4 (below) we see that the grid potential considerably controls the incorporated charge. For high positive grid voltages $V_G = +1000$ V we get a plus–minus–plus–minus charge distribution instead of a minus-plus-minus one obtaines for lower V_G. Also the range of incorporated charges is increasing with V_G. That indicates that the surface potential V_0 has become more positive and the incident beam energy is increased by $+eV_0$.

Generally we may state that the actual retarded or elevated electron beam energy $E_0^|$ is diminished or increased by the surface potential V_0

$$E_0^| = E_0 + eV_0 \tag{7}$$

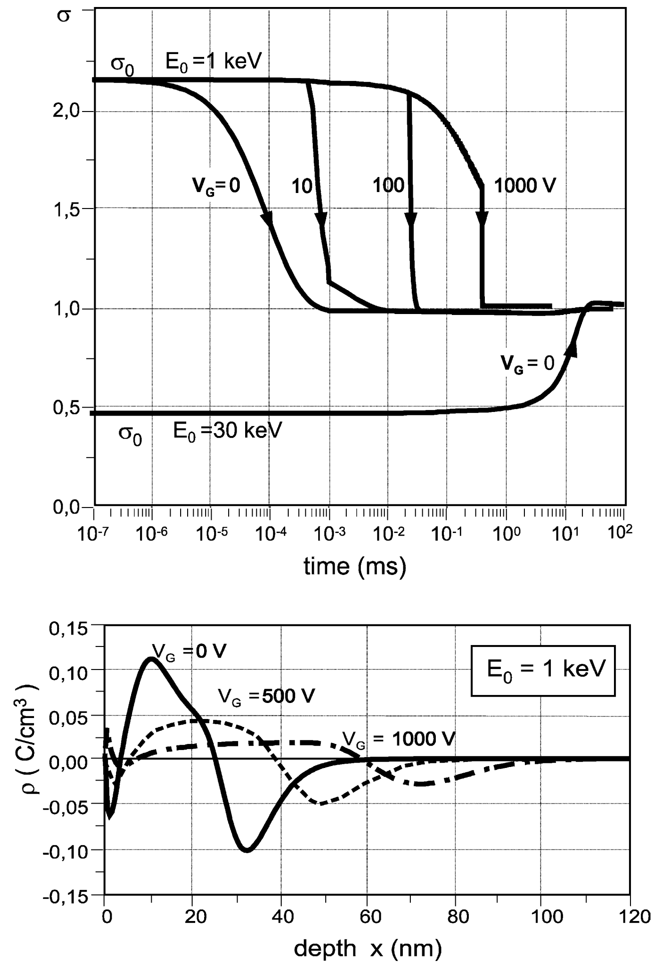

Fig. 4. Rapid change of the secondary electron emission fraction $\sigma = \eta + \delta$ from a 3 mm Al_2O_3 sample with irradiation time t for $E_0 = 1$ and 30 keV, respectively, and different external grid potentials V_G; The initial value σ_0 $(t \to 0)$ corresponds to the non-charged sample; the final steady state for the bulk sample should always approach $\sigma = 1$ (above); Final steady state charge distributions $\rho(x)$ for the low energy injection $E_0 = 1$ keV and different external grid potentials V_G (below) ($j_0 = 10^{-5}$ A/cm^2).

Thus, let us check experimentally the surface potential $V_0(x = 0)$. We will use the X-ray brems-strahlung (BS) spectra, i.e. the shift of the short wavelength threshold due to the negative surface potential V_0 and respective retarding of the PE beam according to Eq. (7). This method has been proposed already by other authors, e.g. Belhaj et al.[11] In Fig. 5 this effect is demonstrated for the bulk 3 mm Al_2O_3 sample and $E_0 = 30$ keV electron beam irradiation. We observe the BS short wave limit at $E_x = 13$ keV; that corresponds to a negative surface potential of $V_0^{exp} = -17$ kV. Comparing this with our simulation value of $V_0 = -21$ kV from[8] we recognize a worse isolation behavior of the real experimental Al_2O_3 target than of the simulated one. Indeed, this was expected and, nevertheless, it demonstrates the right tendency of huge negative charging for high electron beam energies with secondary electron rates $\sigma(E_0) < 1$ and bulk insulating samples.

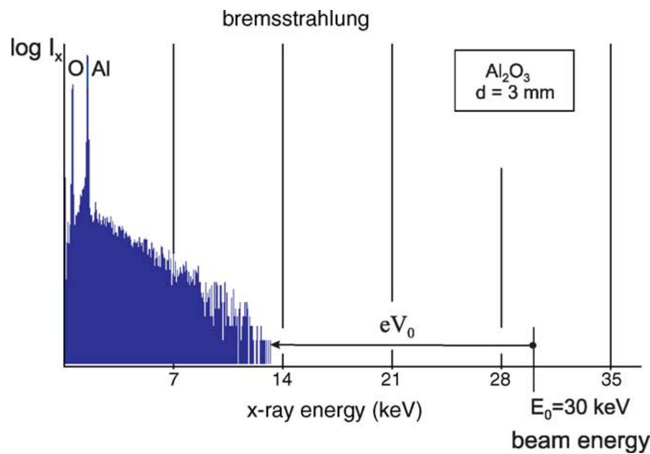

Fig. 5. Measurement of the negative surface potential V_0 by means of the EDX bremsstrahlung (BS) spectra and the high energy (short wavelength) threshold shift: $E_x^{|} = E_0 + eV_0$. We obtain an experimental value of $V_0 = -17$ kV with respect to the computed value of -21 kV.

4. Conclusions

The selfconsistent charge transport in thin silica films and bulk alumina samples during electron beam irradiation is described by means of an iterative computer simulation. Ballistic electron and hole transport as well as their recombination and trapping are included. As a main result the time dependent secondary electron emission rate $\sigma(t)$ and the spatial distributions of currents $j(x, t)$, charges $\rho(x, t)$, the field $F(x, t)$ and the potential slope $V(x, t)$ are obtained. For bulk insulating samples the time-dependent distributions approach the final stationary state with $j(x, t) = \text{constant} = 0$ and $\sigma = 1$. Especially for low electron beam energies $E_0 = 1$ keV the incorporation of charges can be controlled by the potential V_G of a vacuum electrode in front of the target surface.

Finally, for high electron beam energies and bulk samples, the real negative surface potential $V_0 < 0$ is measured by EDX bremsstrahlung spectra and the shift of the short wavelength edge. For the initial beam energy $E_0 = 30$ keV the experimental value $V_0 = -17$ kV is still in agreement with the simulation of an ideal target providing a higher value of $V_0 = -21$ kV.

References

1. *Fourth International Conference on Electric Charges in Non-Conductive Materials* (*Vol Special CSC'4*), Le Vide: Science, Techniques et Applications, 2001.
2. Blaise, G. and Sarjeant, W. J., *IEEE Trans. Dielectr. Electr. Insulat.*, 1998, **5**, 779–808.
3. Levy, L., *Material Charging*. Cedapus, 2002, pp. 241–266.
4. Griseri, V., Levy, L., Payan, D., Maeno, T., Fukunaga, K. and Laurent, C., In *Conference on Electrical Insulation and Dielectric Phenomena, IEEE Transactions on Dielectrics and Electrical Insulation (Annual Report)*, 2002, pp. 922–925.
5. Fitting, H.-J., Schreiber, E., Kuhr, J.-Ch. and Czarnowski, A. vo n, Attenuation and escape depths of low energy electron emission. *J. Electron. Spectrosc. Relat. Phenom.*, 2001, **119**, 35–47.
6. Schreiber, E. and Fitting, H.-J., Monte Carlo simulation of secondary electron emission from the insulator SiO_2. *J. Electron. Spectrosc. Relat. Phenom.*, 2002, **124**, 25–37.
7. Glavatskikh, I. A., Kortov, V. S. and Fitting, H.-J., Self-consistent electrical charging of insulating layers and metal-insulator-semiconductor structures. *J. Appl. Phys.*, 2001, **89**, 440–448.
8. Meyza, X., Goeuriot, D., Guerret-Piécourt, C., Tréheux, D. and Fitting, H.-J., Secondary electron emission and self-consistent charge transport and storage in bulk insulators: application to alumina. *J. Appl. Phys.*, 2003, **94**, 5384–5392.
9. Hingst, Th., Hübner, M., Franz, R., Kuhr, Ch. and Fitting, H.-J., High-field EBIC by computer controlling. *Microelectron. Eng.*, 1994, **24**, 181–188.
10. Fitting, H.-J., Glaefeke, H., Wild, W., Franke, M. and Müller, W., Elektronenstrahlinduzierter Ladungstransport in SiO_2-Schichten. *Experimentelle Technik der Physik*, 1979, **27**, 13–24.
11. Belhaj, M., Ibara, O., Filippov, M. N., Rau, E. I. and Andrianov, M. V., *Appl. Surf. Sci.*, 2001, **177**, 58–65.